TRANSNAV
http://www.transnav.eu
the International Journal
on Marine Navigation
and Safety of Sea Transportation
Volume 12
Number 4
December 2018
DOI: 10.12716/1001.12.04.14

Numerical Study of Hydrodynamic Derivatives and Course Stability under Ship-Bank Interaction

H. Liu, N. Ma & X.C. Gu
Shanghai Jiao Tong University, Shanghai, China

ABSTRACT: Since ship-bank interaction affects the manoeuvrability of a ship navigating close to a bank, the determination of hydrodynamic derivatives is of great importance to assess the ship manoeuvrability. To obtain the hydrodynamic derivatives of the KVLCC2 model ship with different water depths and ship-bank distances, the simulation of PMM tests are carried out using an unsteady Reynolds-Averaged Navier–Stokes (RANS) based solver. Hybrid dynamic mesh technique is proposed to realize the simulation of pure yaw tests in confined water. Studies on the grid convergence and time-step-size convergence are firstly performed. Hydrodynamic derivatives for the ship in different water depths and ship-bank distances are compared. The course stability is investigated based on time-domain simulations and eigenvalue analysis, and the results show that the ship-bank interaction and shallow water effect have a remarkable influence on the course stability.

1 INTRODUCTION

The ship-bank interaction, which is also referred to as bank effects, often leads to a suction force towards the bank and a bow-out or bow-in moment. Therefore it significantly increases the risk of collision against the bank or passing ships. For navigation safety concern, investigating the manoeuvrability of a ship influenced by ship-bank hydrodynamic interaction is of importance. During the past decades researchers have been focusing on providing suitable formulations to predict bank-induced lateral force and yaw moment according to extensive experimental results (Norrbin 1974, Ch'ng et al. 1993, Li et al. 2003, Lataire and Vantorre 2008). On the other hand, the role of hydrodynamic derivatives in evaluating the manoeuvrability of the ships close to banks was discussed in recent papers. Sano et al. (2014) presented the variation of hydrodynamic derivatives with the ship speed, water depth and off-centreline displacement and the consequent change of course stability based on their captive model tests. Liu et al. (2016) carried out a series of planar motion mechanism (PMM) tests in a Circulating Water Channel (CWC) to study the impact of ship-bank interaction on the manoeuvring performance of a VLCC ship model.

Nowadays researchers resort to using computational fluid dynamics (CFD) to deal with the problem of ship-bank interaction. Zou and Larsson (2013) utilized a Reynold-averaged Navier Stokes (RANS) solver to study the bank effects on a tanker hull that proceeds in different canals. Hoydonck et al. (2015) applied several CFD methods to predict the loads on the KVLCC2 Moeri tanker for varying depths and positions in a channel. In order to determine the hydrodynamic derivatives through virtual test technology, Mucha and el Moctar (2013) conducted the simulations of PMM tests for KVLCC2 tanker with various distances to a vertical bank. To generate the time-varying computational grids for the

dynamic motion of PMM tests, methods such as dynamic layering combined with sliding interface (Yang 2011) and tetrahedral grid remeshing (Pan et al. 2012) have been used in the past. However, these methods require enough space between the ship and the boundaries of the computational domain for remeshing, thus they are incapable of simulating the motion in confined water.

In this paper, the hybrid dynamic mesh technique is proposed to solve the problem of remeshing in confined computational domain. The uncertainties relating to grid and time-step discretization are quantified. A series of calculations is conducted for the PMM tests with different water depths and ship-bank distances. The first-order derivatives are obtained and the change of the derivatives with water depth and ship-bank distance are presented. The course keeping performance under ship-bank interaction is simulated in time domain and the course stability is evaluated by eigenvalue analysis.

2 MANOEUVRING FORMULATION

2.1 *Maneuvering theory*

The coordinate system used for all numerical simulations in this paper is shown in Figure 1. Both the earth-fixed coordinate system $O_0\xi\eta\zeta$ and ship fixed coordinate system $Oxyz$ are a right-handed coordinate system with the positive ζ and z axis pointing into the page and the origin O set at the mid-ship point. The ship is expected to move in the direction of the ξ axis at speed U. Affected by the suction force and yaw moment from the bank effect, the ship's velocity vector is [u, v, r] and a heading angle ψ appears between ξ axis and x axis. Consequently a rudder deflection δ is needed to keep the ship's original course, which can be also described by the distance between ship and bank, y_{bank}.

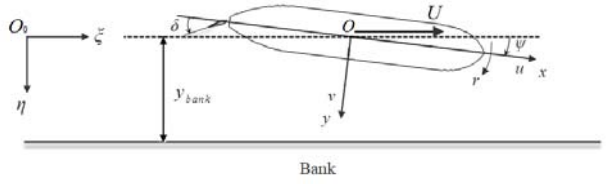

Figure 1. Coordinate systems.

The problem of ship manoeuvring close to a bank features a small deviation in sway and yaw motion and the ship speed is assumed constant, i.e. $u \approx U$. Therefore the equation of surge motion is neglected and the equations of ship motion are given as

$$m\left(\dot{v}+ur+x_G\dot{r}\right)=Y \tag{1}$$

$$I_z\dot{r}+mx_G\left(\dot{v}+ur\right)=N \tag{2}$$

where m is the ship mass, I_z is the moment of inertia about the z axis and Y and N are the external sway force and yaw moment acting on the ship, respectively. All variables are transferred to non-dimensional values with respect to the ship length L, draft T, ship speed U and water density ρ through the equations as follows:

$$\begin{aligned} &m'=\frac{m}{0.5\rho L^2T},\ I_z'=\frac{I_z}{0.5\rho L^4T},\ \dot{v}'=\frac{\dot{v}L}{U^2},\ \dot{r}'=\frac{\dot{r}L^2}{U^2}\\ &u'=\frac{u}{U},\ v'=\frac{v}{U},\ r'=\frac{rL}{U},\ \eta'=\frac{\eta}{L},\ x_G'=\frac{x_G}{L}\\ &Y'=\frac{Y}{0.5\rho LTU^2},\ N'=\frac{N}{0.5\rho L^2TU^2} \end{aligned} \tag{3}$$

Assuming small deviations in sway and yaw motion, the total sway force and yaw moment acting on the ship are expressed as the polynomials of first-order hydrodynamic derivatives and bank induced interaction forces.

$$Y'=Y_{\dot{v}}'\dot{v}'+Y_{\dot{r}}'\dot{r}'+Y_v'v'+Y_r'r'+Y_{bank}'+Y_\delta'\delta \tag{4}$$

$$N'=N_{\dot{v}}'\dot{v}'+N_{\dot{r}}'\dot{r}'+N_v'v'+N_r'r'+N_{bank}'+N_\delta'\delta \tag{5}$$

In Equations 4 and 5, the linear velocity (Y_v', N_v') and acceleration ($Y_{\dot{v}}'$, $N_{\dot{v}}'$) derivatives are determined by a pure sway test and the rotational (Y_r', N_r') and angular acceleration ($Y_{\dot{r}}'$, $N_{\dot{r}}'$) derivatives are determined by a pure yaw test. The derivatives for bank induced forces (Y_{bank}', N_{bank}') and the rudder control derivatives (Y_δ', N_δ') are measured through the rudder angle tests, where the value of the fitted curve of Y' and N' at δ=0 refer to Y_{bank}' and N_{bank}'. For a detailed explanation of the approaches to identify the derivatives, the readers are referred to Yoon et al. (2015). Substituting Equations 4 and 5 into the non-dimensional form of Equations 1 and 2 results in the following equations:

$$\begin{aligned} &\left(m'-Y_{\dot{v}}'\right)\dot{v}'-Y_v'v'+\left(m'x_G'-Y_{\dot{r}}'\right)\dot{r}'+\left(m'-Y_r'\right)r'\\ &=Y_\delta'\delta+Y_{bank}' \end{aligned} \tag{6}$$

$$\begin{aligned} &\left(m'x_G'-N_{\dot{v}}'\right)\dot{v}'-N_v'v'+\left(I_z'-N_{\dot{r}}'\right)\dot{r}'+\left(m'x_G'-N_r'\right)r'\\ &=N_\delta'\delta+N_{bank}' \end{aligned} \tag{7}$$

2.2 *Course stability analysis*

The course (directional) stability is particularly important for a ship sailing under bank effect. In practice, a ship is stable if a disturbance applied to deflect the ship from its current course, results in the ship eventually resuming a new straight line after the disturbance disappears (Kobylinski 2003). For ships near banks, rudder forces are first used to counteract the interaction force. After a ship reaches motion equilibrium, the course stability can be judged according to the eigenvalues of the homogeneous form of Equations 6 and 7.

In this study, the pole placement method (Kautsky et al. 1985) is adopted to control the rudder angle

before the motion equilibrium is achieved. Firstly Equations 6 and 7 are rearranged with respect to $[v\ r]^T$, yielding the state equations as follows:

$$\mathbf{M}\begin{bmatrix}\dot{v}'\\ \dot{r}'\end{bmatrix}+\mathbf{N}\begin{bmatrix}v'\\ r'\end{bmatrix}=\mathbf{F}_R\begin{bmatrix}\delta\end{bmatrix}+\mathbf{F}_B \tag{8}$$

where

$$\mathbf{M}=\begin{bmatrix}-Y'_{\dot{v}}+m' & -Y'_{\dot{r}}+m'x'_G\\ -N'_{\dot{v}}+m'x'_G & -N'_{\dot{r}}+I'_z\end{bmatrix}$$
$$\mathbf{N}=\begin{bmatrix}-Y'_v & -Y'_r+m'\\ -N'_v & -N_r+m'x'_G\end{bmatrix} \tag{9}$$
$$\mathbf{F}_R=\begin{bmatrix}Y'_\delta\\ N'_\delta\end{bmatrix}\quad \mathbf{F}_B=\begin{bmatrix}Y'_{bank}\\ N'_{bank}\end{bmatrix}$$

Then, the state vector $[v\ r]^T$ is expanded by adding the cross track error y and the heading angle ψ which satisfy:

$$\dot{y}'=v'\cos\psi+u'\sin\psi=v'+\psi \tag{10}$$

$$\dot{\psi}'=r' \tag{11}$$

The final state-space equations are given as:

$$\begin{bmatrix}\dot{v}'\\ \dot{r}'\\ \dot{\psi}'\\ \dot{y}'\end{bmatrix}=\begin{bmatrix}-\mathbf{M}^{-1}\mathbf{N} & \begin{matrix}0&0\\0&0\end{matrix}\\ \begin{matrix}0&1\\1&0\end{matrix} & \begin{matrix}0&0\\1&0\end{matrix}\end{bmatrix}\begin{bmatrix}v'\\ r'\\ \psi\\ y'\end{bmatrix}+\mathbf{M}^{-1}\begin{bmatrix}\mathbf{F}_R\delta & \mathbf{F}_B\\ 0&0\\0&0\end{bmatrix} \tag{12}$$

The input variable in the linear system of Equation 12 is the rudder angle. In order to complete a closed loop, the input in Equation 12 is expected to be given as $\mathbf{u}=-\mathbf{K}\mathbf{x}$. Here the pole placement is used to compute the gain matrix $\mathbf{K}$ that can ensure the poles of the closed-loop system at the desired locations. The time-domain computation of Equation 12 will end up with a steady ruder angle δ and a heading angle ψ. At this phase the right-hand side of Equations 6 and 7 becomes zero. Then, the ship's motion variables v' and r' due to a small disturbance are defined as:

$$v'=C_1e^{\sigma t},\qquad r'=C_2e^{\sigma t} \tag{13}$$

where C_1 and C_2 are arbitrary variables. By substituting Equation 13 into Equations 6 and 7, the characteristic equation is written as:

$$A\sigma^2+B\sigma+C=0 \tag{14}$$

where

$$\begin{aligned}A&=\left(m'-Y'_{\dot{v}}\right)\left(I'_z-N'_{\dot{r}}\right)-\left(m'x'_G-N'_{\dot{v}}\right)\left(m'x'_G-Y'_{\dot{r}}\right)\\ B&=-Y'_v\left(I'_z-N'_{\dot{r}}\right)+N'_v\left(m'x'_G-Y'_{\dot{r}}\right)\\ &+\left(m'-Y'_{\dot{v}}\right)\left(m'x'_G-N'_r\right)-\left(m'x'_G-N'_{\dot{v}}\right)\left(m'-X'_{\dot{u}}-Y'_r\right)\\ C&=-Y'_v\left(m'x'_G-N'_r\right)+N'_v\left(m'-X'_{\dot{u}}-Y'_r\right)\end{aligned} \tag{15}$$

To ensure the ship's course stability, the following Hurwitz stability criterion (Bergmann 1964) should be satisfied, meaning that Equation 9 has negative real roots only:

$$A>0,\ B>0,\ C>0\ \text{ or }\ A<0,\ B<0,\ C<0 \tag{16}$$

Since $\left(m'-Y'_{\dot{v}}\right)$, $\left(I'_z-N'_{\dot{r}}\right)$ and $-Y'_v$ are always larger positive values than other terms in Equations 6 and 7, it can be concluded that $A>0$, $B>0$ is ensured for most ships. Therefore, the criterion can be reduced to $C>0$.

3 NUMERICAL SIMULATION METHOD

3.1 *Numerical method*

The simulations of PMM tests are performed with the Reynolds-averaged Navier-Stokes (RANS) equations in the CFD software ANSYS FLUENT. The flow is defined as single-phase, 3-D and incompressible viscous flow. The flow model is implicit unsteady with a segregated predictor-corrector solver. Semi-Implicit Method for Pressure-Linked Equations-Corrected (SIMPLEC) algorithm is applied to solve the velocity-pressure coupling. The RNG k-ε turbulence model by Yakhot and Orszag (1986) is introduced to close the RANS equations.

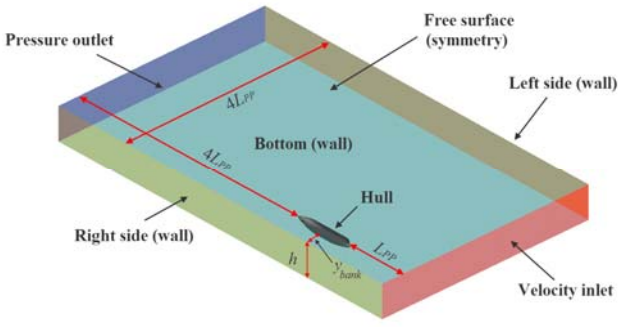

Figure 2. Computational domain and boundaries.

The computational domain and boundary conditions for PMM simulation is set as illustrated in Figure 2. It extends 4.0 L_{PP} (L_{PP} is the length between perpendiculars) from the aft to the pressure outlet, 1.0 L_{PP} from the bow to the velocity inlet. The breadth of the domain is 4.0 L_{PP}, while the length of y_{bank} from starboard to the right side wall is varied. The depth h between the free surface and the bottom is also alterable. Due to the low Froude number (F_r=0.066 based on L_{PP}), the free surface is considered rigid as symmetry boundary.

A hybrid dynamic mesh technique is proposed to simulate the pure yaw motion near the bank. As Fig.3 shows, the whole computational domain is divided into three parts. The internal region is meshed with

tetrahedral cells, and the external and stationary region are swept with prismatic cells. The pure yaw motion is decomposed into transverse movement (pure sway) and horizontal rotation. The pure sway is realized in the external region by layering method, and the rotation is completed in the internal region by local remeshing. The distribution of grids follows the rule that cells located in the internal region is around 60-70 percent and 10-15 percent in the external region and 20-25 percent in the stationary region. The dynamic and stationary regions are separated by grid interfaces. All the mesh motion at each time step is programmed by User Defined Functions (UDF).

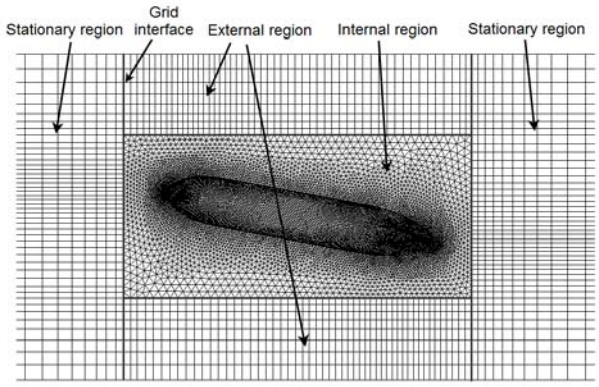

Figure 3. Hybrid grid regions for pure yaw test simulation.

3.2 *Convergence study on grid and time step size*

The specific case for the presented study is known as the KVLCC2 Moeri tanker. The model data are published via (SIMMAN 2008). The principal particulars of the KVLCC2 test model together with the full scale ship are listed in Table 1.

Table 1. Principle dimensions of the KVLCC2

Parameters	Full scale	Model
Length between perpendiculars L m	320.00	2.4850
Breadth B m	58.00	0.4504
Design draft T m	20.80	0.1615
Displacement ∆ m3	312540	0.1464
LCB from Mid-ship xB m	11.04	0.086
Scale	128.77:1	

The convergence study follows the methodology adopted in the International Towing Tank Conference (ITTC) recommended procedures for the uncertainty analysis in CFD (ITTC 2002). This paper focuses on the verification work in the recommended procedures, which is applied to assess the numerical uncertainty in the simulations with gradually refined grids and time steps. Firstly, the grid-convergence study focuses on the simulation of pure sway test. Three sets of grid are generated with the grid refinement conforming to a uniform refinement ratio $r_G = \sqrt[4]{2}$. The grid volume of the three sets, namely Grid 1, Grid 2 and Grid3 is respectively 2656360, 1681260 and 1016970. The values of the derivatives from pure sway motion (symbolized as S_1, S_2 and S_3 in terms of grid volume) are selected as the objects for uncertainty estimation and shown in Table 2 The changes between S_1, S_2 and S_3 are given by $\varepsilon_{21} = S_2 - S_1$ and $\varepsilon_{32} = S_3 - S_2$, and the grid convergence ratio R_G are obtained by $R_G = \varepsilon_{21}/\varepsilon_{32}$. The numerical uncertainty of grid size U_G can be calculated through a complex derivation, for which the readers refer to (ITTC 2002). In Table 2, the monotonic convergence appears in $Y'_{\dot{v}}$ and $N'_{\dot{v}}$ with $0 < R_G < 1$ while oscillatory convergence appears in Y'_v and N'_v with $R_G < 0$. The uncertainty U_G can be estimated in both conditions and the results (presented as the percentage of the derivatives for Grid 1) show that the numerical uncertainty in terms of grid number is fairly small. Grid 2 is chosen in the subsequent simulation for computational efficiency.

Table 2. Results of grid convergence study

	$Y'_{\dot{v}}$	Y'_v	$N'_{\dot{v}}$	N'_v
Grid 1	-0.3275	-0.1611	-0.5064	-0.0209
Grid 2	-0.3296	-0.1620	-0.5064	-0.0206
Grid 3	-0.3342	-0.1606	-0.5062	-0.0210
R_G	0.4785	-0.6272	0.2753	-0.7785
U_G	0.00848	0.00069	0.00021	0.00020
U_G (% Grid 1)	2.59%	0.43%	0.04%	0.96%

Secondly, the time step convergence is checked by using three time steps Δt =0.007s, 0.01s and 0.014s and the Grid 2 to simulate the same pure sway case as the grid convergence study. The results of the derivatives with the corresponding convergence ratio R_T and uncertainty U_T are listed in Table 3. The numerical uncertainties in terms of time step are smaller and Δt =0.01s is chosen to simulate further cases of pure sway. The time steps for pure yaw test is set Δt =0.003s because the smaller step is needed to avoid negative-volume cells' appearance during the remeshing.

Table 3. Results of time step convergence study

	$Y'_{\dot{v}}$	Y'_v	$N'_{\dot{v}}$	N'_v
Δt=0.007s	-0.3299	-0.1618	-0.5063	-0.0205
Δt =0.01s	-0.3296	-0.1620	-0.5064	-0.0206
Δt=0.014s	-0.3292	-0.1622	-0.5079	-0.0207
R_T	0.5118	0.7472	0.0543	0.6316
U_T	0.00022	0.00052	0.00016	0.00017
U_T (% Δt =0.007s)	0.07%	0.32%	0.03%	0.81%

4 RESULTS AND DISCUSSION

4.1 *Hydrodynamic derivatives*

The types of PMM test include pure sway test, pure yaw test and rudder angle test, covering a series of ship-bank distance to breadth ratios y_{bank}/B =2.8, 1.7 and 1.35, and water depth to draft ratios h/T=1.2, 1.5 and 10. The velocity inlet speed is set at U=0.326m/s (F_r=0.066) that is 35 percent of the service speed.

Figure 3 and 4 show the derivatives versus h/T at y_{bank}=1.7B as well as the derivatives versus y_{bank}/B at h=1.2T. To compare the derivatives under bank effect with respect to the derivatives in open water with infinite depth, the condition of y_{bank} = 10B and h=10T was simulated additionally, of which the derivatives are marked as "Deep open water". It can be seen the magnitudes of most derivatives except Y'_r and N'_r

are larger in confined water than the derivatives in deep open water.

The absolute values of $Y'_{\dot{v}}$, $N'_{\dot{r}}$ and $Y'_{\dot{r}}$ increase at shallow water depth. They correspond to added mass and added moment of inertia with a change of sign. Therefore the ship sailing in shallow water needs longer time to change its state of motion than in deep water. An exceptional case is the oscillation of $N'_{\dot{v}}$ that is mainly due to the change of grid distribution in the case of shallow water. Since the value of $N'_{\dot{v}}$ is relatively small, the accuracy of $N'_{\dot{v}}$ by CFD is not as good as other derivatives. For velocity derivatives and rotational derivatives, the magnitudes of Y'_v and N'_v rise strikingly with the decreasing h/T while N'_r appears an opposite trend. And the value of Y'_r oscillates with h/T.

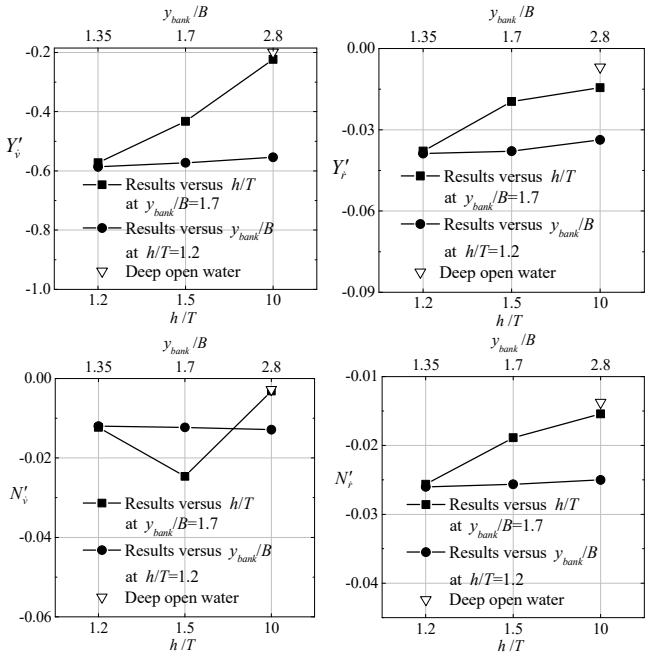

Figure 3. Acceleration derivatives versus ybank/B and h/T.

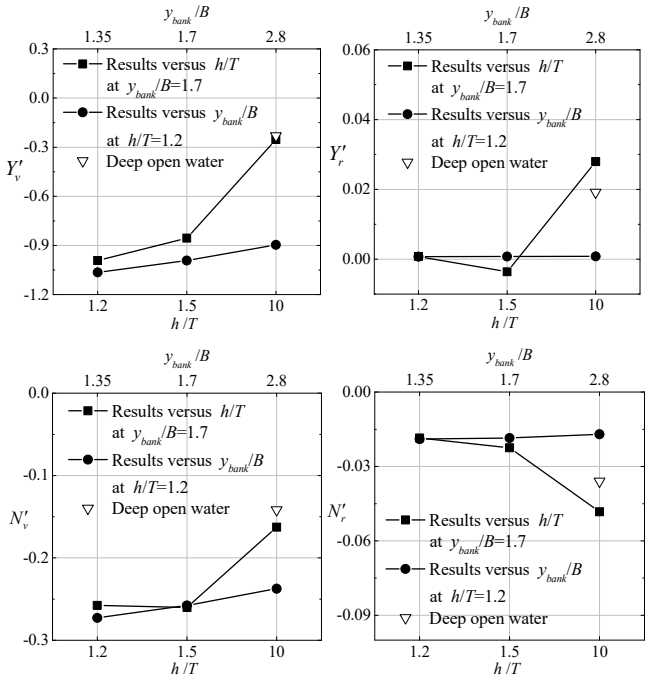

Figure 4. Velocity derivatives versus y_{bank}/B and h/T.

As to the results versus y_{bank}/B at h=1.2T, the magnitudes of acceleration derivatives increase with the decreasing ship-bank distance except $N'_{\dot{v}}$ which shows a slight downtrend. The similar trend appears in the velocity and rotational derivatives. The values of Y'_v, Y'_r, N'_v and N'_r refer to a push-out force and a bow-out moment on the moving ship caused by v and r respectively. It indicates that the hydrodynamic forces are enhanced by the ship-bank interaction.

The fitting curves of the rudder force and moment versus the rudder angle with different ship-bank distances at h/T=1.2 are shown in Figure 5. The curves have apparent asymmetries with respect to the origin point, which means the ship-bank interaction exerts a suction force and a bow-out moment on the ship. The rudder derivatives Y'_δ and N'_δ plotted in Figure 6 do not show significant changes in different ship-bank distances.

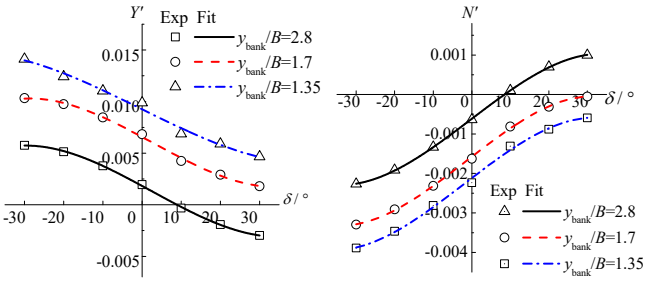

Figure 5. Rudder force and moment versus δ with variations in y_{bank}/B.

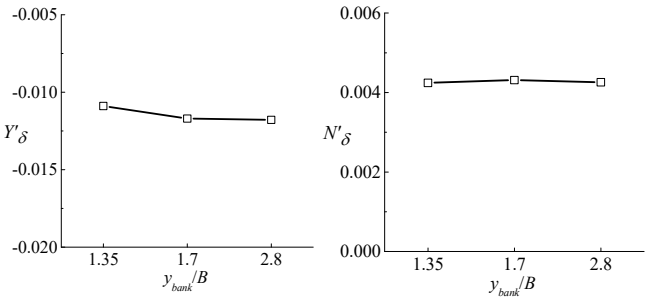

Figure 6. Rudder derivatives versus y_{bank}/B.

4.2 *Course stability*

The course keeping performance using the pole placement control is simulated for different water depths and ship-bank distances. The poles are chosen to -0.5, -16.1 and -2.4±0.16i and found from repeated tests. The simulation is performed for the speed corresponding to F_r=0.066 and the rudder deflection and steering velocity followed by the control law is controlled with 35° and 7.6°/s.

Figure 7 shows the results of course control with variations in water depth. The initial position of the ship is at y_{bank}=2.5B, and the positive y/B means the ship is closer to the bank. The ship moves to the bank at the start phase. Then, the rudder angle grows drastically to change the ship's direction to "away from the bank". A negative heading angle is generated to give a Munk moment to counteract the rudder forces. Finally, the ship reaches the motion equilibrium before t=20s. The rudder angle and the

overshoot of y/B increase as the water becomes shallower in general. The largest overshoot of y/B appears at h=1.5T. It shows that the shallow water effect enhances the ship-bank interaction and a larger rudder deflection is needed to keep course. However, at h=1.2T the situation may not be even worse.

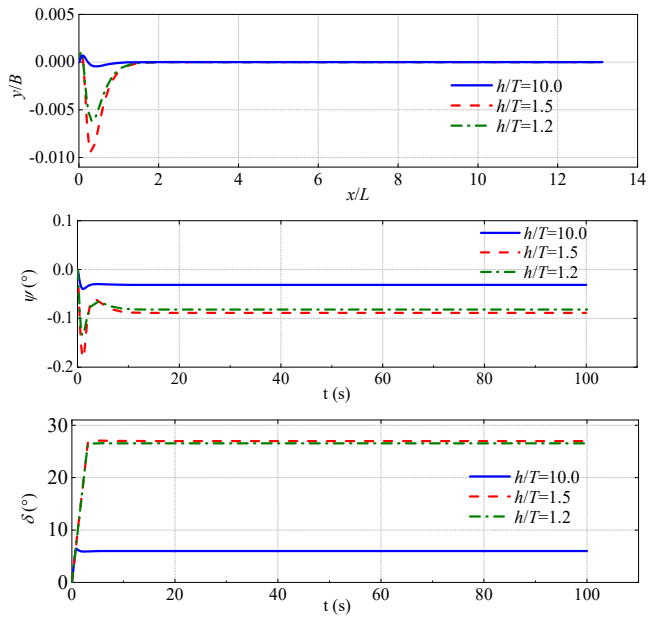

Figure 7. Time traces of course control with various h/T.

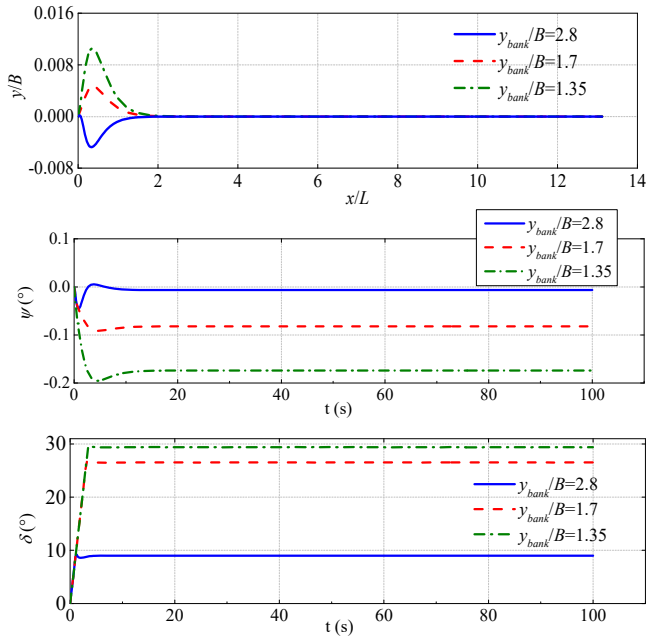

Figure 8. Time traces of course control with various y_{bank}/B.

Figure 8 shows the ship-bank distance has the significant effect on the results of course keeping control. The simulation is conducted at h=1.2T with the ship initially placed at y_{bank}=2.8B, 1.7B and 1.35B. Due to the increasing suction force by the bank, the cross track error tends to be closer to the bank when y_{bank} reduces to 1.7B. Consequently, larger rudder deflection is required for the equilibrium of motion when the ship is very close to the bank. The rudder angle needed to achieve the equilibrium at h=1.2T and y_{bank}=1.35B is nearly 30°. Also, the reverse heading angle grows from -0.1° to -0.2°. Since the ship's deviation from the initial path is quite small in Figures 7 and 8, the control system following pole placement method manifest its advantage of offering large control inputs to counteract the ship-bank interaction.

Based on the sign of parameters of A, B and C calculated by Equation 15, the course stability of the ship after the disturbance disappears in proximity to a bank can be discussed. Figure 9 presents the values of A, B and C versus h/T and y_{bank}/B. For all the cases, A and B are positive but C is negative. This implies that the ship is unable to keep a straight line if no control action is taken after the disturbance. C for shallow water conditions is much more negative than it is for h=10T, which indicates the shallow water effect makes this problem even worse.

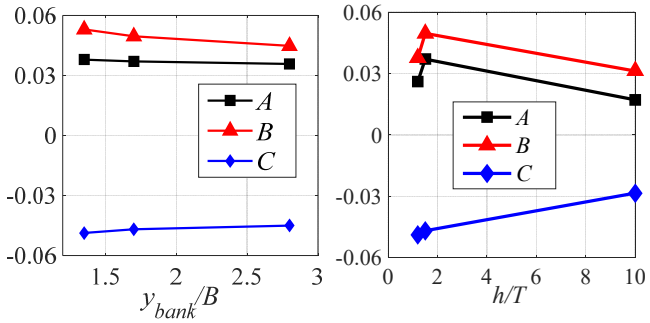

Figure 9. Parameters A, B and C versus h/T and y_{bank}/B.

5 CONCLUSIONS

The present study applies CFD method to simulate the PMM tests of KVLCC2 model ship with variations in water depth and ship-bank distance, and investigates the change of hydrodynamic derivatives and course stability for the ship. The hybrid dynamic mesh method is developed to solve the problem of mesh configuration and remeshing in limited space. Validation study is performed through the convergence study of grid and time step. Further calculation results show that shallow water effect enlarges the value of hydrodynamic derivatives, and the magnitudes of derivatives mostly increases with the decrease of ship-bank distance. The pole placement method is capable of controlling the KVLCC2 to achieve the equilibrium of motion in different water depths and ship-bank distances. Large rudder deflections are necessary to achieve the motion equilibrium in shallow water and "very close to bank" conditions e.g. h=1.2T and y_{bank}=1.35B. The course stability analysis indicates that the ship is unstable without control and the shallow water condition can worsen this problem.

ACKNOWLEDGEMENT

The research is supported by the China Ministry of Education Key Research Project "KSHIP-II Project" (Knowledge-based Ship Design Hyper-Integrated Platform): No. GKZY010004.

REFERENCES

Bergmann H. G. 1964. On the conditions under which an equation has only roots with negative real parts. *Selected Papers on Mathematical Trends in Control Theory*: 70–82. New York: Dover, USA.

Ch'ng P. W., Doctors L. J., Renilson M. R. 1993. A method of calculating the ship-bank interaction forces and moments in restricted water. *International Shipbuilding Progress*, 40(421): 7−23.

Hoydonck W. van, Toxopeus S. L., Eloot K., et al. 2015. Bank Effects for KVLCC2. *Proceedings of World Maritime Technology Conference 2015 (WMTC 2015)*. Providence, RI, USA.

ITTC. 2002. CFD General Uncertainty Analysis in CFD Verification and Validation Methodology and Procedures. Recommanded Procedures 7.5 -03-01-01.

Kautsky J., Nichols N. K., Van Dooren. P. 1985. Robust pole assignment in linear feedback. *International Journal of Control*, 41(5): 1129-1155.

Kobylinski L. K. 2003. Directional stability of ships and safe handling. *Marine Technology V*.

Lataire E., Vantorre M. 2008. Ship-bank interaction induced by irregular bank geometries. *Proceedings of the 27th symposium on naval hydrodynamics*: 511–524. Seoul, Korea.

Lataire E., Vantorre M., Delefortrie, G. 2012. A prediction method for squat in restricted and unrestricted rectangular fairways. *Ocean Engineering*, 55(55): 71-80.

Li D. Q., Ottosson P., Tragardh P. 2003. Prediction of bank effects by model tests and mathematical models. *Proc. MARSIM'03, International Conference on Marine Simulation and Ship Maneuverability*: RC30. 1−12. Kanazawa, Japan.

Liu H., Ma N., Gu X. C. 2016. Ship–bank interaction of a VLCC ship model and related course-keeping control. *Ships and Offshore Structures*, 12(s1): 306-316.

Mucha, P., el Moctar, O. 2013. Ship-Bank interaction of a large tanker and related control problems. *Proc. of the 32nd ASME International Conference on Ocean, Offshore and Arctic Engineering (OMAE 2013)*. Nantes, France.

Norrbin, N. H. 1974. Bank effects on a ship moving through a short dredged channel. *Proceedings of the 10th Symposium on Naval Hydrodynamics*: 71−87. Cambridge, USA.

Pan Y. C., Zhang H. X., Zhou Q. D. 2012. Numerical prediction of submarine hydrodynamic coefficients using CFD simulation. *Journal of Hydrodynamics, Ser. B*, 24(6): 840-847.

Sano, M., Yasukawa, H., Hata, H. 2014. Directional stability of a ship in close proximity to channel wall. *Journal of Marine Science and Technology* 19(4): 376-393.

SIMMAN 2008. MOERI Tanker (KVLCC2). 2008. http://www.simman2008.dk/KVLCC/KVLCC2/tanker2.html.

Yakhot V., Orszag, S. A. 1986. Renormalization group analysis of turbulence. I. Basic theory. *Journal of Scientific Computing*, 1(1): 3−51.

Yang Y. 2011. Calculation of Unsteady Hydrodynamic Forces on a Maneuvering Ship. Master thesis, Shanghai Jiao Tong University, Shanghai.

Yoon H., Simonsen C. D., Benedetti L., Longo J., Toda Y., Stern F. 2015. Benchmark CFD validation data for surface combatant 5415 in PMM maneuvers – Part I: Force/moment/motion measurements. *Ocean Engineering*, 109:705-734.

Zou L., Larsson L. 2013. Computational fluid dynamics (CFD) prediction of bank effects including verification and validation. *Journal of Marine Science and Technology*, 18(3): 310-323.